Ziegler, M., Reiter, K., Heidbach, O., Zang, A., Kwiatek, G., Stromeyer, D., Dahm, T., Dresen, G., Hofmann, G. (2015):Mining-Induced Stress Transfer and Its Relation to a Mw 1.9 Seismic Event in an Ultra-deep South African Gold Mine. - *Pure and Applied Geophysics*, *172*, 10, pp. 2557—2570.

DOI: http://doi.org/10.1007/s00024-015-1033-x

Pure and Applied Geophysics manuscript No.
(will be inserted by the editor)

Mining-induced stress transfer and its relation to a M_w 1.9 seismic event in an ultra-deep South African gold mine

Moritz Ziegler ·
Karsten Reiter ·
Oliver Heidbach ·
Arno Zang ·
Grzegorz Kwiatek ·
Dietrich Stromeyer ·
Torsten Dahm ·
Georg Dresen ·
Gerhard Hofmann

Published online: 01 February 2015
The final publication is available at Springer via
http://dx.doi.org/10.1007/s00024-015-1033-x

Abstract On 27 December 2007 a M_w 1.9 seismic event occurred within a dyke in the deep level Mponeng gold mine, South Africa. From the seismological network of the mine and the one from the JAGUARS group, the hypocentral depth (3509 m), focal mechanism and aftershock location was estimated. Since no mining activity took place in the days before the event, dynamic triggering due to blasting can be ruled out as the cause. To investigate the hypothesis that stress transfer, due to excavation of the gold reef, induced the event, we set up a small scale ($450 \times 300 \times 310\,m^3$) high resolution 3D geomechanical-numerical model. The model consists of the four different rock units present in the mine: quartzite (footwall), hard lava (hanging wall), conglomerate (gold reef), and diorite (dykes). The numerical solution is computed with a finite element method, with a discretised mesh of approximately 10^6 elements. The initial stress state of the model is in agreement with in-situ data from a neighbouring mine and the step-wise excavation is simulated by mass removal from the gold reef. The resulting 3D stress tensor and its changes due to mining is analysed with the Coulomb failure stress changes on the fault plane of the event. The results show that the seismic event was induced regardless of how the Coulomb failure stress changes are calculated and of the uncertainties of the fault plane solution. We also use the model to assess the seismic hazard due to the excavation towards the dyke. The resulting curve of stress changes shows a significant increase in the last ∼50 m in front of the dyke indicating that small changes in the mining progress towards the dyke have a substantial impact on the stress transfer.

Keywords induced seismicity · static stress change · deep level mining · tabular mining · Coulomb failure stress · 3D geomechanical numerical model

M. Ziegler · K. Reiter · O. Heidbach · A. Zang · G. Kwiatek · D. Stromeyer · T. Dahm · G. Dresen
Helmholtz Centre, GFZ German Research Centre for Geosciences, Telegrafenberg, 14473 Potsdam, Germany
E-mail: mziegler@gfz-potsdam.de

M. Ziegler · K. Reiter · A. Zang · T. Dahm · G. Dresen
University of Potsdam, Institure of Earth and Environmental Science, Karl-Liebknecht-Str. 24-25, 14476 Potsdam-Golm, Germany

G. Hofmann
Anglogold Ashanti, 76 Jeppe Street, Newtown, Johannesburg, 2001, South Africa

1 Introduction

Seismicity in mining environments can cause large damages (McGarr 1971; Ortlepp 1992, 2001; Brady & Brown 2004; Orlecka-Sikora *et al.* 2012; Hasegawa *et al.* 1989; Pytel 2003). Especially in deep-level high-stress environments, such as the South African Gauteng mining district, seismicity induced by mining excavations is a high risk (Prinsloo 2011; Pretorius 1976; Gay & Ortlepp 1979; Hofmann *et al.* 2013). There the vertical stress due to the overburden reaches values of 80–100 MPa (Lucier *et al.* 2009). Furthermore, inhomogeneities like variable rock strength, paleosurfaces, inherited fault zones or intrusions can act as promoter for violent failure of rocks (Pretorius 1976; Gay & Ortlepp 1979).

On 27 December 2007, an M_w 1.9 seismic event occurred in the ultra-deep levels of Mponeng tabular gold mine, Carletonville, South Africa (Yabe *et al.* 2009; Plenkers *et al.* 2010; Naoi *et al.* 2011; Kwiatek *et al.* 2010; Kwiatek & Ben-Zion 2013). The hypocentre and its aftershocks were located within a dyke at an approximate depth of 3509 m in direct proximity (<50 m) to access tunnels and recently mined-out areas of the gold bearing target horizon (Kwiatek *et al.* 2010; Naoi *et al.* 2011; Kwiatek & Ben-Zion 2013). Since the seismic event occurred on the fifth day of the Christmas closure of the mine, the level of background noise due to excavation work was low, which allows for a precise detection and location of the aftershocks (Plenkers *et al.* 2010). Furthermore, dynamic triggering of the event by blasting activities can be ruled out and hence the event was most likely induced by stress transfer due to the excavation towards the dyke in the preceding months. Hofmann *et al.* (2012) investigated whether the event was induced by stress changes by means of a homogeneous elastic boundary element model. From their model they estimated the excess

shear stress (ESS),

$$ESS = |\tau| - \mu\sigma_n \quad (1)$$

which is defined as the difference between normal stress σ_n multiplied with the internal friction coefficient μ and the absolute value of the shear stress τ prior to slip for a given fault orientation (Ryder 1988). Hofmann *et al.* (2012) estimated the plane which is optimally oriented in the stress field after excavation from a grid search and found that its orientation is similar to the rupture plane of the event estimated by Naoi *et al.* (2011) and the aftershock distribution. From these results they concluded that the event was induced by the excavation of the gold reef.

In this paper, we also investigate whether the event was induced by stress transfer, but instead of the ESS value we use two versions of the change of Coulomb failure stress (ΔCFS) analysis to investigate in detail which component of the stress transfer is the potential key driver for the event. The ΔCFS is defined as

$$\Delta CFS = \Delta\tau - \mu\Delta\sigma_n \quad (2)$$

the difference between the normal stress σ_n multiplied with the friction coefficient μ and the shear stress component τ in slip direction (rake) of the seismic event prior to slip for a given fault (e.g. King *et al.* 1994; Harris 1998; Stein 1999; Heidbach & Ben-Avraham 2007). In addition to this definition we also calculate the ΔCFS using the maximum shear stress and the ΔCFS values for both nodal planes of the fault plane solution. To simulate the stress changes we use a 3D geomechanical-numerical model that estimates the stress transfer due to step-wise mining excavations immediately before the occurrence of this seismic event. In extension to the model of Hofmann *et al.* (2012) the model area consists of the complex topology of the dyke and the different rock properties of the lithologies are considered.

Since dykes are known to be promoters for failure (Gay & Ortlepp 1979; McGarr *et al.* 1975), we also calculate, in a forward approach, the ΔCFS at the hypocentre of the event. We assume failure on a plane with the orientation of the rupture plane for a semi-generic step-wise excavation towards the dyke. We estimate the variability of the resulting ΔCFS values as a function of excavation distance to the dyke. By varying the orientation of the rupture plane we account for the uncertainties of the fault plane solution. The resulting function can serve as a first-order seismic hazard assessment.

2 Data

2.1 Geological Setting

The Mponeng gold mine represents a typical ultra-deep tabular mining environment (e.g. Hofmann *et al.* 2013; Plenkers *et al.* 2010; Roberts & Schweitzer 1999). It is located in the north-western part of the Witwatersrand Basin, South Africa (Fig. 1) at the centre of the Kaapvaal Craton, which is one of the worlds largest gold mining districts (Coward *et al.* 1995). Mining activity at Mponeng reaches down to about 3900 m (AngloGold Ashanti Limited 2013) and the mine is therefore one of the world's deepest.

Sedimentation in the Witwatersrand Basin started 3086 Ma ago onto 3120 Ma old basement granites and gneiss (Robb *et al.* 1992; Armstrong *et al.* 1991). Over a period of about 1000 Ma, the Witwatersrand-, the Ventersdorp- and the Transvaal Supergroup were deposited (Tab. 1) (Coward *et al.* 1995; Frimmel & Minter 2002).

The meta-sediments of the Mandeor Formation form the model's footwall. They are argillaceous to siliceous quartzites and conglomerates (Roberts & Schweitzer 1999) as well as shale (Jolley *et al.* 2004). In the research area the Mandeor Formation consists of quartzite. The top of the Mandeor Formation is a paleosurface, which has a locally meter-scale slope-terrace relief (Jolley *et al.* 2004). These areas (so called rolls) are frequently subject to violent deformation and fatal mining accidents (Roberts & Schweitzer 1999). The target horizon of the gold exploitation in Mponeng mine is the lowest unit of the Ventersdorp Supergroup, the conglomerate Ventersdorp Contact Reef (VCR) (AngloGold Ashanti Limited 2013). It is made of 1–2 m alluvial coarse conglomerates and quartzites, which lie unconformably above the Mandeor Formation (as a part of the Central Rand Group) (Roberts & Schweitzer 1999). The reef is internally structured into complex terraces and fluvial channels (Frimmel & Minter 2002; Jolley *et al.* 2004) and dips with $\sim 22^\circ$ to the SSE (e.g. Hofmann *et al.* 2013; Plenkers *et al.* 2010). The enrichment of the gold took place during fluvial transport and eolian upgrading (deflation) as well as due to post-sedimentary hydrothermal displacement (Frimmel & Minter 2002). Large mafic to komatiitic flood basalts with mantle origin (Alberton metabasalts/hard lava) were deposited above the VCR with thicknesses of up to 2000 m (Van der Westhuizen *et al.* 1991). After the deposition of the Transvaal Supergroup, two events overprinted the region. First, the Bushveld Igneous Complex, which is related to thermal metamorphism due to mafic underplating of the lower crust, and second the Vredefort impact event, which led to the formation of the Vredefort Dome (Coward *et al.* 1995; Frimmel & Minter 2002). Both are believed to be responsible for hydrothermal alteration (e.g. gold enrichment within the reef) and many intrusions (e.g. the Pink-Green and Great-Green Dyke) in Witwatersrand Basin (Coward *et al.* 1995; Frimmel & Minter 2002).

Fault ramps are restricted to the footwall, forming fault-bend folds and imbricated zones close to the VCR and detach the footwall from the hanging wall below or within the VCR (Jolley *et al.* 2004). This is mainly observed in the

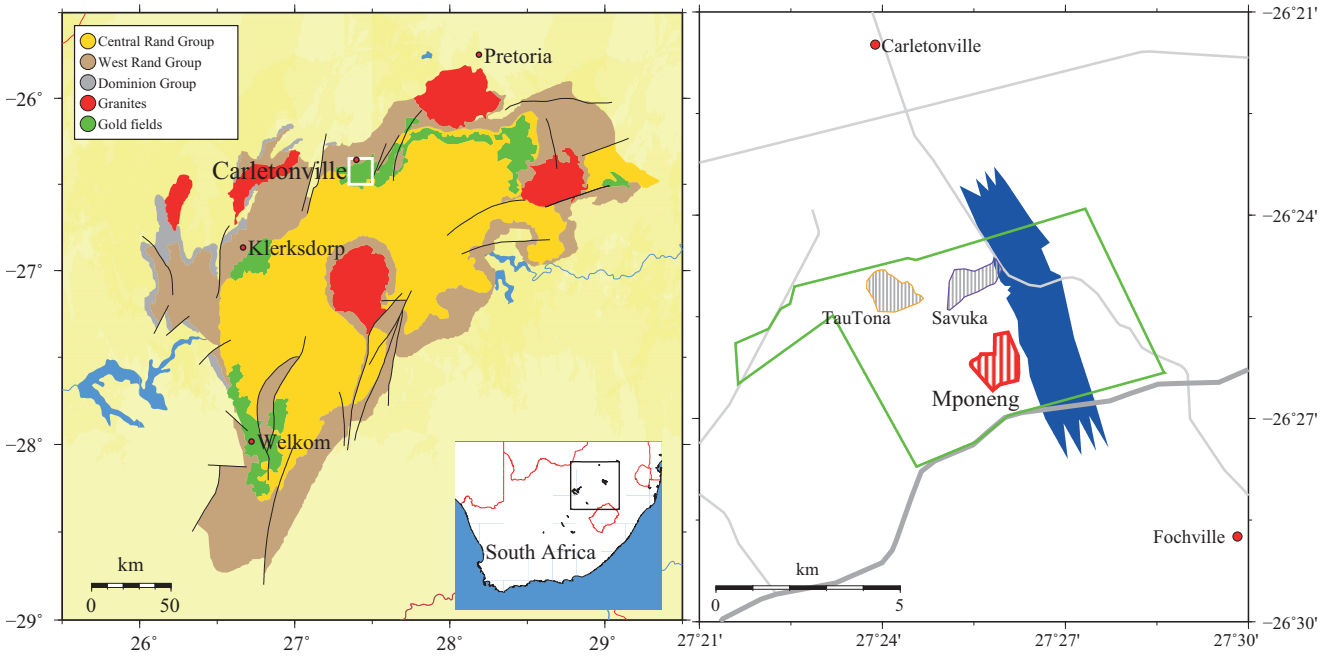

Fig. 1 Left: The Witwatersrand Basin and its geological units. The white box indicates the location of the right map section. Right: The mining area around Carletonville. The borders of AngloGold Ashanti's claim (green), known occurrence of Booysens shale of the Mandeor Formation (blue), major roads (grey), and the surface operations of the three mines.

Table 1 Stratigraphic table of the units and area of interest for the model of the Mponeng gold mine in Witwatersrand Basin, South Africa.

Supergroup	Group	Formation	age [Ma]	Relevance for the model
Vredefort impact			2023[a]	Peak metamorphism & hydrothermal alteration
Bushveld Igneous Complex			2054[b]	of VCR, dyke intrusion?
Transvaal			2250[a] 2642[c]	
Ventersdorp	Pniel Sequence Platberg		2709[d]	
	Klipriviersberg	Alberton Venterpost	2714[d] 2714[e]	hard lava (hanging wall) Ventersdorp Contact reef (VCR)
Witwatersrand	Central Rand	Mandeor	2837[a]	quartzite (footwall)
			<2894[f]	
	West Rand		2914[d] <2970[a]	
	Dominion		3074[d] 3086[g]	
Basement			3120[d]	

[a]Frimmel & Minter (2002), [b]Scoates & Friedman (2008), [c]Eriksson *et al.* (1995),[d]Armstrong *et al.* (1991), [e]Hall *et al.* (1997), [f]Poujol *et al.* (1999), [g]Robb *et al.* (1992)

eastern part of the mine, where Booysens Shale (Fig. 1) underlies the reef (Jolley *et al.* 2004) and hence it is not in the model area. The highest gold contents are observed along such imbrications and associated with transfer faults, which have Klipriviersberg ages (Jolley *et al.* 2004). Two subvertical intrusions, the mafic Pink-Green and Great-Green dyke, cross the research area in NNW and NNE direction (Kwiatek *et al.* 2010). They probably intruded in post Transvaal time (Pretorius 1976). The hypocentre of the M_w 1.9 seismic event is located within the Pink-Green dyke (Fig. 2) (Yabe *et al.* 2009; Plenkers *et al.* 2010; Kwiatek & Ben-Zion 2013; Hofmann *et al.* 2012, 2013).

2.2 The M_w 1.9 seismic event

On 27 December 2007 an M_w 1.9 seismic event occurred in the deep level of Mponeng gold mine at ∼3509 m during the mine's Christmas holidays (Plenkers *et al.* 2010; Naoi *et al.* 2011; Kwiatek & Ben-Zion 2013). During the Christmas closure of the mine there was a low level of background noise (no blasting or movement of heavy equipment). These circumstances rule out dynamic triggering and allowed undisturbed recording of the aftershock sequence which contain valuable information (Kwiatek *et al.* 2010; Plenkers *et al.* 2010).

Due to wrong polaritiy of the seismometer channels and maintenance issues, only 9 out of 27 stations of the mine's network could be used for the estimation of the focal mech-

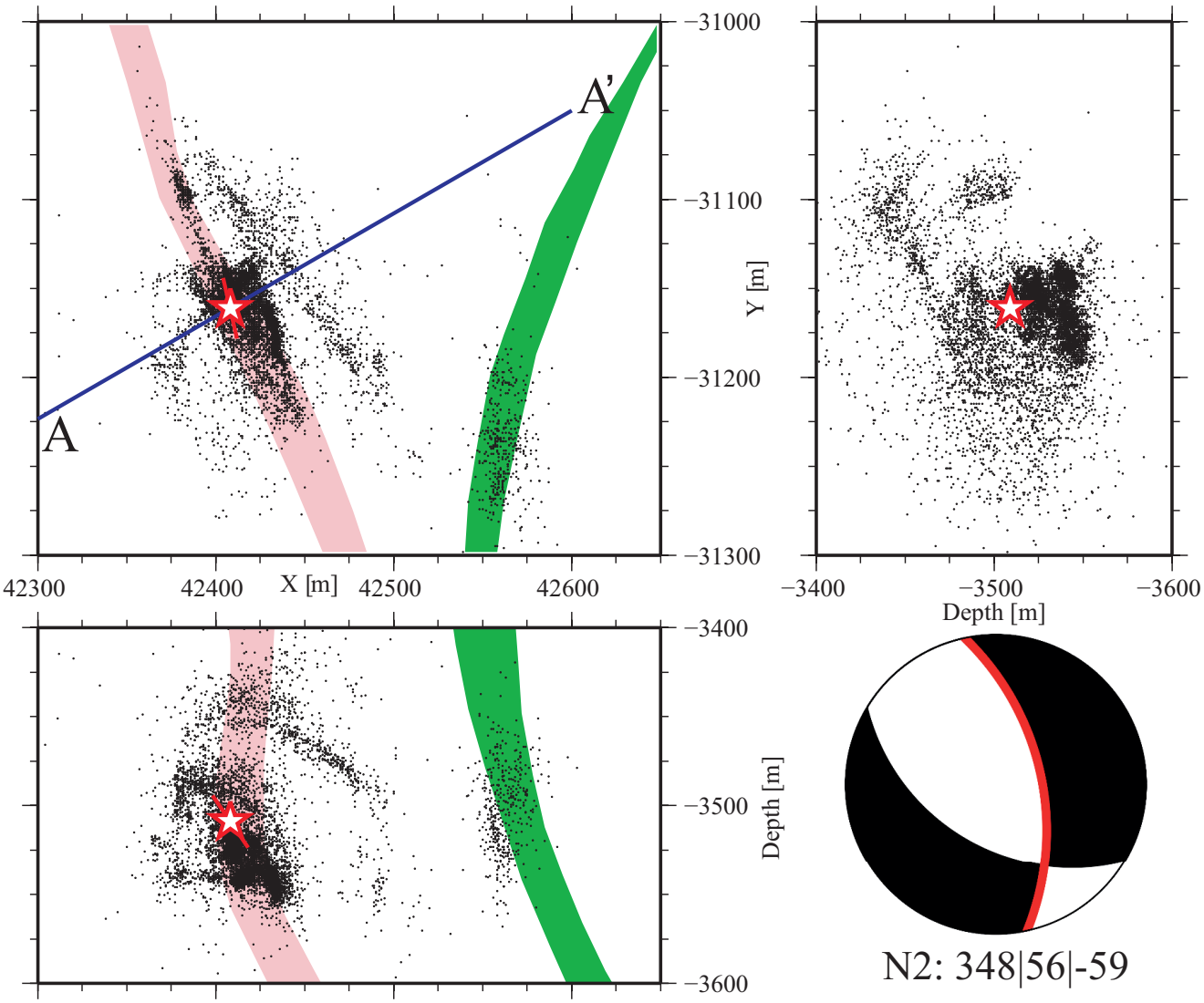

Fig. 2 The distribution of aftershocks in map view (top left) and two depth sections (cumulative along the map area). The star marks the hypocentre of the M_w 1.9 main shock. The approximate extent (pink and green) of the two dykes at focal depth are displayed. The blue line A–A' indicates a transect (Fig. 3) which is approximately perpendicular to the strike of the preferred nodal plane (red line, the rupture length (∼35 m), derived from empirical relations (Leonard 2010)) Bottom right: Focal mechanism of the M_w 1.9 main shock with the preferred nodal plane N2 in red. (Naoi *et al.* 2011; Kwiatek & Ben-Zion 2013)

anism solution (Naoi *et al.* 2011). The focal mechanism solution displayed in Figure 2 shows a normal faulting regime with the two nodal planes N1: 125|46|-129 (strike|dip|rake) and N2: 348|56|-59 as expected (Naoi *et al.* 2011; Kwiatek & Ben-Zion 2013). The aftershocks of the main event were recorded at a distance of ∼30 m to the hypocentre by the high frequency acoustic emission sensor JAGUARS-network (Japanese-German Underground Acoustic Emission Research in South Africa) (Naoi *et al.* 2008; Nakatani *et al.* 2008; Plenkers *et al.* 2010). This network registered more than 20 000 aftershocks with magnitudes as small as -4.4 (Fig. 2) (Kwiatek *et al.* 2010; Plenkers *et al.* 2010; Naoi *et al.* 2011). The distribution of aftershocks presented in Figure 3 indicates that the nodal plane N2 (348|56|-59) is the rupture plane (Naoi *et al.* 2011; Kwiatek & Ben-Zion 2013). Furthermore, the normal faulting mechanism of the event is in agreement with the in-situ stress field (Lucier *et al.* 2009) and the generally expected mechanisms of mining seismicity (Horner & Hasegawa 1978, in Hasegawa *et al.* 1989; Gay & Ortlepp 1979; Aswegen 2008).

3 Model description

To estimate the stress state and its changes due to the stepwise excavation of the gold reef immediately before the seismic event, we set up a 3D geomechanical-numerical model that simulates the excavation work of the mine and the subsequent stress transfer. The computed induced stress changes

are then inspected for their potential to cause the M_w 1.9 seismic event. In this section the model assumptions, boundary conditions, material properties and initial stress conditions are presented.

3.1 Assumptions

In the process of model-building, we made the following assumptions concerning the model's properties and considered processes:

1. Dynamic triggering: No blasting was performed at the time and the days before the M_w 1.9 event due to the Christmas holidays (Hofmann *et al.* 2012; Plenkers *et al.* 2010). Thus, dynamic triggering can be ruled out.
2. Thermal stresses: The temperature at focal depth is $\sim$ 60°C (Jones 1988). The air temperature in the mine is cooled down to about 35°–40°C. The thermal stresses induced by the mentioned temperature change in the vicinity of the hypocentre are negligibly small. Due to the small thermal diffusivity of the rock significant thermal stresses can only be expected in direct proximity (few meters) to the excavated and cooled areas during the observed time frame. The hypocentre lies in a distance from the cooled areas where thermal stresses can be neglected.
3. Backfill and support pillars: A slurry of waste material is pumped into the mined out areas (Lucier et al. 2009). However, the rigidity (Young's modulus) of this backfill is three magnitudes smaller than the mined out rock (E=16 GPa) (Lucier *et al.* 2009) and thus the impact of the backfilling it is not regarded. Also the impact of the pillars that support the roof of the mined out areas on the stress field is very local and small and thus can also be neglected. All the same in terms of roof stability pillars are most significant.
4. Gravity acceleration: We assume gravitational body forces of 9.79 m/s^2 adapted to the depth and a local anomaly (Lindau 2007). Details on the implementation of the initial load due to gravity are presented in the following Section 3.2.
5. Rheology: We assume linear elastic rock properties in each material block (gold reef, dykes and host rock) with the values stated in Table 2. To account for plastic processes in the near-field of the excavation area, in particular the roof and the front of the mined out region (Malan 1999), we assume in one version of the model result analysis that all horizontal stress components do not contribute to the stress changes in the dyke. Thus we consider two end member cases: The first assumes that stresses are transferred into the dyke by elastic response only. The second case assumes that all horizontal stresses are dissipated by local plastic processes (failure) in the excavation damage zone (EDZ). The latter implies that only the change of the overburden (σ_v component in Fig. 4) controls the stress changes in the dyke.

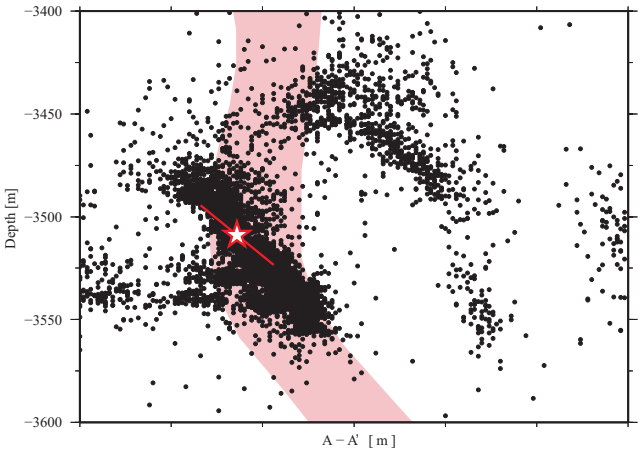

Fig. 3 The aftershocks and the main shock (star) are projected onto the transect A–A' (blue line in Fig 2). The abscissa (A' is in direction of 70°) is approximately perpendicular to the strike direction of the nodal plane N2 (strike: 348°). An accumulation of aftershocks can be observed close to the hypocentre of the main shock on a plane dipping similar to the nodal plane N2 (dip: 56°, red line, the rupture length ($\sim$35 m), derived from empirical relations (Leonard 2010)).

3.2 Model formulation, parameters and solution

With the stated assumptions the problem can be formulated with the partial differential equation of the equilibrium of forces. The stress changes will follow from the deformation that results from the excavation as indicated in the sketch of Figure 4. These are equilibrated with the initial load due to gravity. Given the complexity of the 3D geometry and the inhomogeneous distribution of material properties, we use a Finite Element Method (FEM) to solve the problem numerically at discrete points. The FEM with its unstructured mesh allows the discretisation of a volume with a high resolution in the area of interest and a coarse mesh further away (Fig. 5). This enables a beneficiary trade-off between spatial resolution and computational time. Furthermore, the FEM is capable of resembling the irregular shapes of the tunnel system, dykes and the thin gold reef. The different rock properties of each lithology (Tab. 2) are assigned to the corresponding elements.

3.3 Model geometry, discretisation, boundary and initial conditions

The model volume of $450 \times 300 \times 310\,\mathrm{m}^3$ is only a small part of the mine. It is located around the hypocentre of the

Table 2 Elastic material properties and density applied in the model.

Component	Lithology	Young's modulus [GPa]	Poisson ratio	Density [kg/m^3]
Dykes	Diorite[f]/Gabbro[b]	110[c]	0.25[d,e]	2900[b,e]
Hanging Wall	Hard lava[a]	88[a]	0.26[a]	2902[a]
VCR (Gold reef)	Quartz pebble conglomerate[b]	69[b]	0.20[b]	2600[c]
Footwall	Quartzite[a,f]	79[a]	0.13[a,e]	2710[a,e]

[a]Malan (1999), [b]Gay (1979), [c]MatWeb LLC (2013), [d]Gercek (2007), [e]S. Stanchits (pers. comm.), [f]Stanchits *et al.* (2010)

M_w 1.9 seismic event. The information on the geometrical and structural features, in particular the irregular shape of the dykes, were provided by the mining company. To ensure that the final discretisation of the volume is sufficiently detailed and to avoid numerical errors, we performed a series of 2D resolution test models (not shown in this paper). The final 3D mesh (Fig. 5) consists of $\sim 10^6$ finite elements (tetrahedrons and hexahedrons) with linear approximation functions.

The initial load due to the overburden and the tectonic stresses are implemented with appropriate kinematic boundary conditions. They are determined in such a way that they represent the in-situ stress data from the neighbouring TauTona mine provided by Lucier *et al.* (2009) which we assume is comparable to the in-situ stress state in Mponeng. The TauTona mine which overlaps the Mponeng mine exploits the Carbon Leader Reef (CLR) which lies about 800 m below the VCR (Lucier *et al.* 2009). Lucier *et al.* (2009) derived the stress state in the NELSAM underground laboratory in TauTona mine. The laboratory is in a vertical distance of 150 m and a horizontal distance of ~2–5 km from the hypocentre in the same footwall rock as Mponeng. Since stresses are continuous, the assumption of a comparable stress state is viable.

Technically we apply a vertical stress of S_v=92 MPa due to the 3380 m overburden on the top of the model. Within the model volume body forces, due to gravity, give an additional vertical stress component. To fit the magnitudes of the maximum and minimum horizontal stresses S_{Hmax} and S_{hmin}, as reported by Lucier *et al.* (2009), we apply appropriate kinematic boundary conditions. The progress of mining excavation is simulated in monthly steps by the removal of material from the gold reef. The static response of the rock is computed in monthly steps as well. The location, geometry and extent of these excavations were provided by the mining company. The removal of the rock material in the initial stress state results in deformations (Fig. 4) and subsequent stress changes in the model volume. The solution of the resulting numerical problem is achieved with the commercial FEM software Abaqus v6.11.

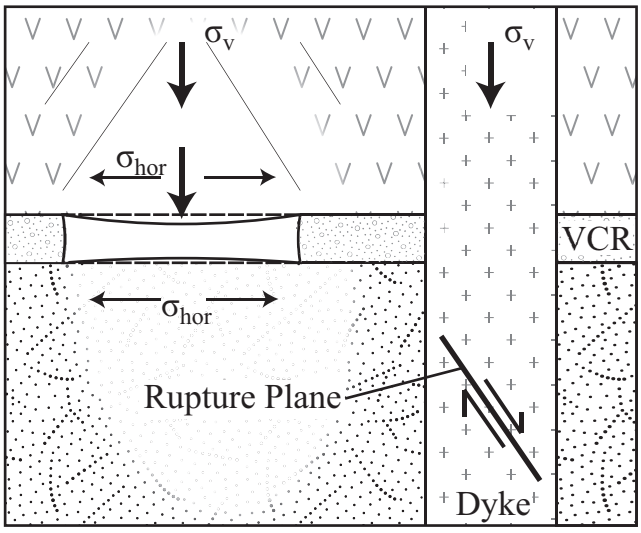

Fig. 4 This sketch shows the response of the rock to excavation in a depth of ~3.5 km. The roof and floor of the excavated section bend inwards and thereby create tensile stresses in the horizontal. At the same time the stress due to the overburden in the mining horizon is redistributed to smaller unmined areas around the dyke. The vertical stress increases significantly in these areas and can ultimately lead to failure in a normal faulting event. Please note that the sketch is not to scale.

4 Analysis of model results

To analyse whether the event was induced by stress changes, we use the change of Coulomb failure stress. The Coulomb failure stress (CFS) is defined as the stress state of a given plane and is expressed by

$$CFS = \tau - \mu\sigma_n \tag{3}$$

where τ is the shear stress, μ the friction coefficient which is usually assumed to be 0.6 (Byerlee 1978) and σ_n the normal stress (King *et al.* 1994; Jaeger *et al.* 2007). For the CFS calculation we use the rupture plane N2 of the M_w 1.9 event with an orientation of 348|56 (strike|dip) (Naoi *et al.* 2011; Kwiatek & Ben-Zion 2013). The changes in CFS (ΔCFS)

$$\Delta CFS = \Delta\tau - \mu\Delta\sigma_n \tag{4}$$

indicate whether a fault is brought closer to (positive ΔCFS value), or further away (negative ΔCFS value) from failure (King *et al.* 1994; Stein 1999). The ΔCFS is calculated by

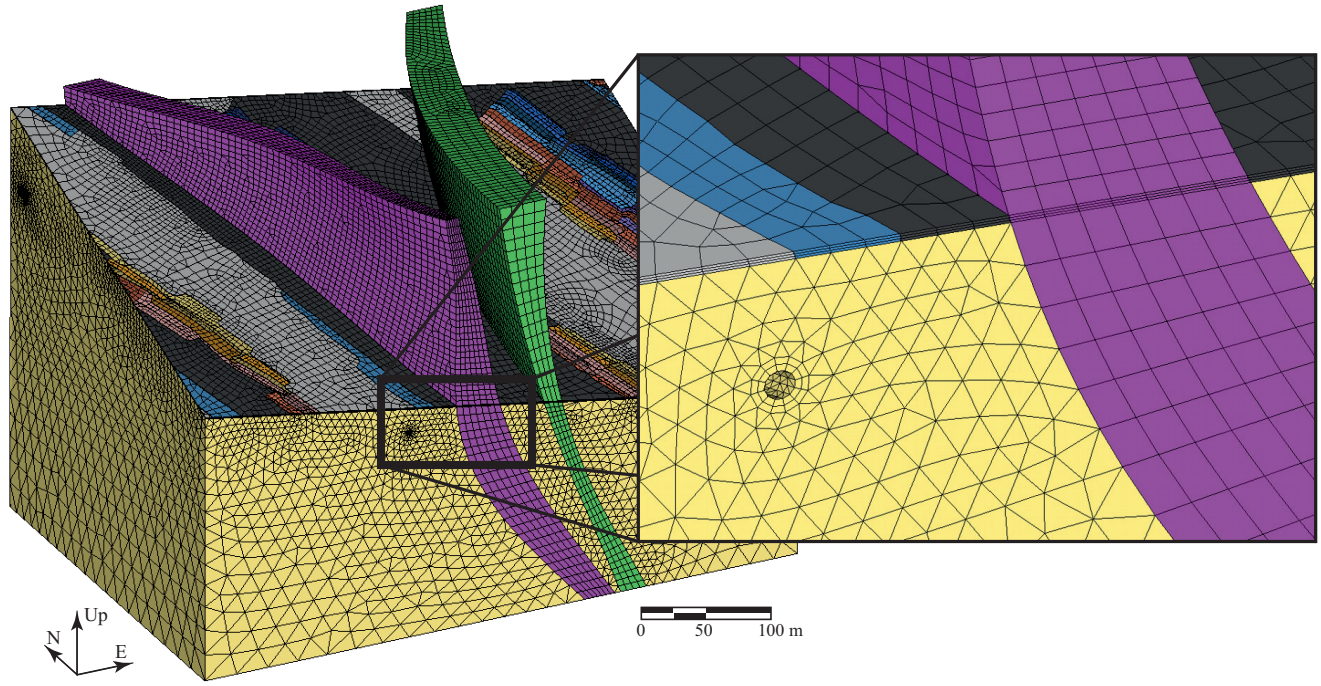

Fig. 5 The discretised geometry of the gold mine. The gold reef (visible top layer) is colour-coded according to the monthly progress of the excavation work. The hanging wall is omitted here to facilitate viewing. Pink-Green Dyke (purple) and Great-Green Dyke (green) are displayed. The mesh contains $\sim 10^6$ hexahedron and tetrahedron elements. The close-up shows the Pink-Green dyke, the thin layered gold reef and the finer discretisation around a mining tunnel. The gold reef is colour coded in grey (mined before 2007), blue (mined in 2007) and black (not mined as of 2009). Y axis points to the north.

the subtraction of CFS of the unmined, initial stress state of the model from the CFS in December 2007, i.e. immediately before the event occurred, but after large amount of rock material was removed. We estimate two different values of ΔCFS; one with the shear stress component resolved in slip direction 348|56|-59 (ΔCFS_{slip}) and the other in direction of maximum shear stress on the rupture plane 348|56 (ΔCFS_{max}). Furthermore, we calculate these two different ΔCFS values for both cases, the elastic response ($\Delta CFS_{slip,el}$, $\Delta CFS_{max,el}$) and the case where we implicitly assume in the analysis that plastic deformation consumes all horizontal stress changes (pseudo-plastic, $\Delta CFS_{slip,pl}$, $\Delta CFS_{max,pl}$).

The results are displayed in 3D (Fig. 6) and cross sections (Fig. 7) for the ΔCFS_{slip} values of the elastic and the pseudo-plastic analysis case using the assumed rupture plane N2 of the focal mechanism solution. Both figures show that the event's hypocentre, which is marked with a white star, is located in an area of positive ΔCFS_{slip}. Table 3 summarises all different ΔCFS values at the hypocentre for the two nodal planes. All values are positive regardless which ΔCFS value and plane is used and they range between 1.57 MPa for $\Delta CFS_{slip,plastic}$ on N1 and 14.77 MPa for $\Delta CFS_{slip,elastic}$ on N1. For the elastic case the difference between the ΔCFS_{max} and ΔCFS_{slip} is relatively small which indicates that the slip vector points in the overall direction of maximum shear stress. The difference between slip direction and direction of maximum shear stress (12°) is caused by the uncertainties in the focal mechanism solution and the uncertainties of the model's geometry. The approximate compliance of the inferred and the maximum slip direction is in agreement with the Bott hypothesis (Bott 1959) that slip occurs in the direction of maximum shear stress. Interestingly, the ΔCFS values for the elastic case are approximately 30 % smaller for the rupture plane N2 compared to the auxiliary plane N1. In contrast to this, the ΔCFS values from the pseudo-plastic case are higher for the N2 plane, i.e. the rupture plane. The absolute numbers for the elastic case and the rupture plane N2 are in overall agreement with the ESS value of $\sim$12 MPa estimated by Hofmann *et al.* (2012).

5 Discussion

5.1 Discussion of the ΔCFS analysis results

The positive changes of all ΔCFS values indicate that the area around the hypocentre of the M_w 1.9 seismic event was brought closer to failure and that the event was most likely induced by the stress changes due to mining. For the elastic case the rupture plane N2 experienced a significantly smaller stress change compared to the auxiliary plane N1 even though N2 was clearly identified as the rupture plane by the distribution of aftershocks. However, this is not necessarily in contradiction with our findings, when we con-

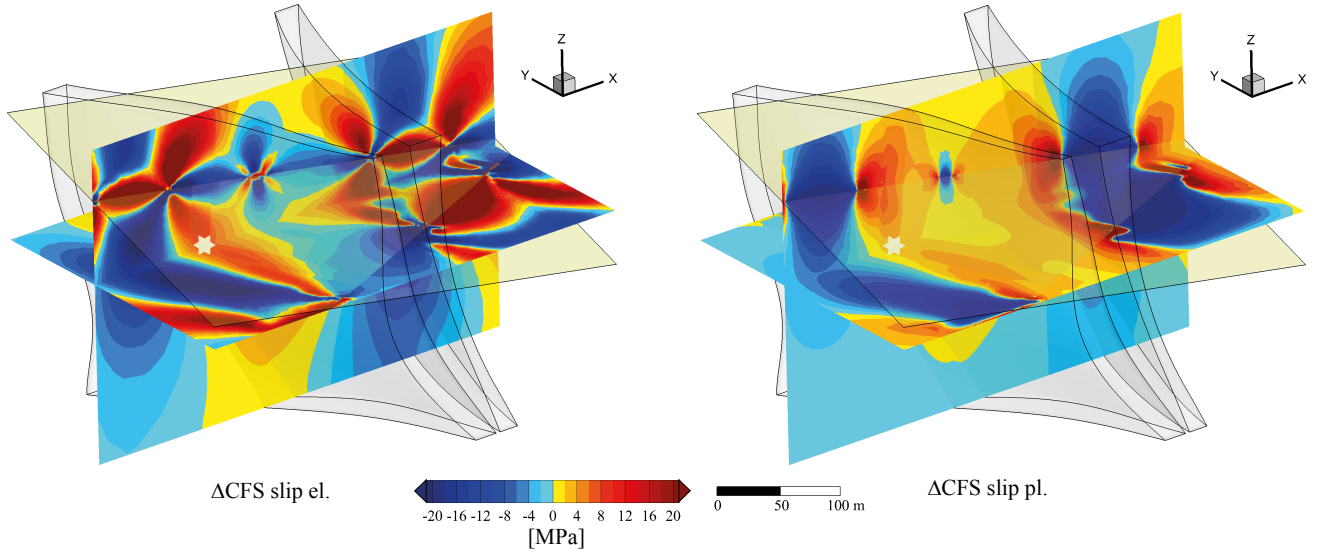

Fig. 6 ΔCFS [MPa] in slip direction (ΔCFS_{slip}) at the time of the M_w 1.9 seismic event derived from the full stress tensor (left) and derived only from the vertical component (σ_v) of the stress tensor, assuming a full dissipation of horizontal stresses (pseudo-plasticity) by local plastic deformation in the excavation damage zone (EDZ) (right). Displayed are two planes that intersect at the hypocentre of the seismic event. Event location is given by the white star. Dykes are the grey compounds and the gold reef is indicated by the yellow dipping plane. Y-axis points to the north. The two planes with ΔCFS are shown in more detail in Figure 7.

Table 3 The results of the different ΔCFS analysis at the hypocentre of the M_w 1.9 seismic event. The nodal plane N2: (348|56| − 59) (Naoi *et al.* 2011) is the rupture plane while N1 is the auxiliary plane. The shear stress in ΔCFS_{slip} is computed in direction of slip, while ΔCFS_{max} utilises the shear stress in the direction of maximum shear stress.

	Elastic		Pseudo-Plastic	
Receiver plane	ΔCFS_{slip}	ΔCFS_{max}	ΔCFS_{slip}	ΔCFS_{max}
N2: (348|56| − 59)	9.85 MPa	9.67 MPa	3.33 MPa	4.38 MPa
N1: (125|46| − 129)	14.77 MPa	14.74 MPa	1.57 MPa	3.33 MPa

sider the slip tendency (ST) value (Morris *et al.* 1996). ST is an absolute measure of how close a fault is to failure and is defined after Morris *et al.* (1996) as:

$$ST = (\tau_{max}/\sigma_n) * \mu^{-1}. \quad (5)$$

Using a friction coefficient of μ=0.6 (Byerlee 1978) the ST value of the initial stress field for N1 is 0.39 and increases due to elastic stress transfer to 0.72 . The ST value of the initial stress field for N2 is 0.45 and increases due to the elastic stress transfer to 0.73. Thus, even though the relative stress transfer to N1 in the elastic analysis is larger than the one on N2, the absolute distance to failure is smaller for plane N2. This demonstrates the challenges of the interpretation of the relative ΔCFS values and the necessity to look at both nodal planes and (if applicable) absolute values like ST. Furthermore, the ST values indicate that even when cohesion is neglected the initial stress state in the dyke is still relatively far away from failure. However, the assumed initial stress field is calibrated against stress data that were not taken from a dyke but from the footwall (Lucier *et al.* 2009). Either in the dyke a pre-existing fault with a lower friction coefficient ($\mu \approx 0.4$) was reactivated or, which is more likely, the initial stresses within the dyke are larger and closer to failure than in intact rock. These higher initial stresses within dykes would exist due to the dyke's higher Young's modulus compared to the host rock (Tab. 2) as well as thermal stresses. The latter are created by the cooling after the dyke's intrusion (Gay 1979; Haxby & Turcotte 1976).

The main sources of uncertainty of the ΔCFS value is the orientation of the fault planes, but moderate deviations of the assumed fault plane in the order of 10°–15° have no significant impact on the overall results of the model. The impact of uncertainties in the geometry of the gold reef, dyke and uncertainty of the material properties on this stress transfer simulation are of minor importance and do not change the general results of the model. Also the numerical error imposed by the linearisation of the problem has been tested and found to be insignificant. In summary this leads to an overall model uncertainty in the order of $\pm$1 MPa.

5.2 Seismic hazard assessment

The previously presented results indicate a high probability that the M_w 1.9 event was induced by mining excavations. The hypocentre of the event was located in a dyke (Plenkers *et al.* 2010; Naoi *et al.* 2008) and dykes are generally

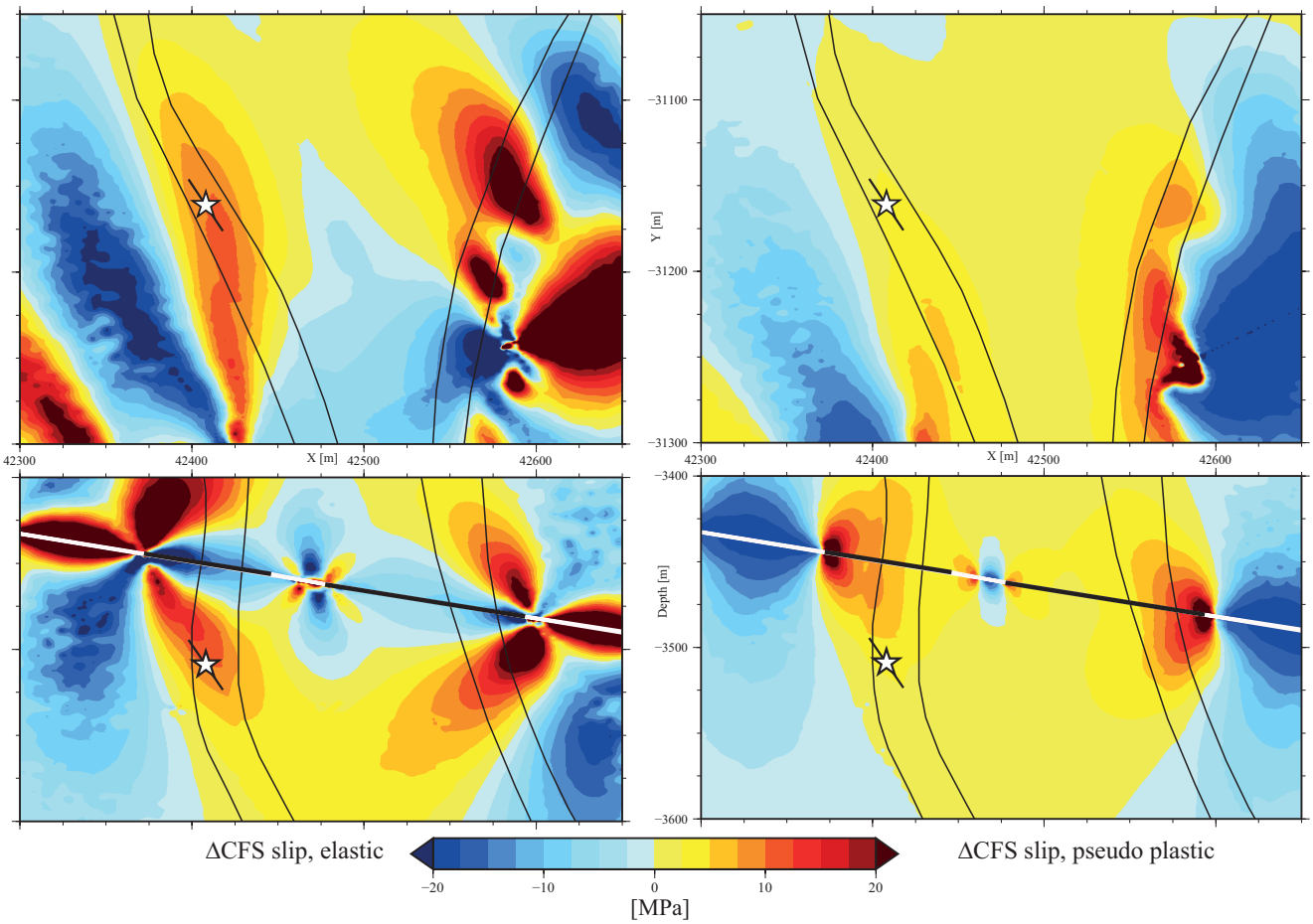

Fig. 7 ΔCFS [MPa] in slip direction (ΔCFS_{slip}) at the time of the M_w 1.9 seismic event derived from the full stress tensor (left) and derived only from the vertical component (σ_v) of the stress tensor, assuming a pseudo-plasticity (right). Horizontal cross sections in depth of the hypocentre (top) and depth sections at $Y = -31160$ m (bottom) of ΔCFS computed for the assumed rupture plane at depth of the hypocentre at the time of the M_w 1.9 seismic event (planes from Fig. 6). The event location is given by the white star; the strike (348°, top) and dip (56°, bottom) of the assumed fault plane is given by the black line (the rupture length of ∼35 m is derived from empirical relations (Leonard 2010)); the dyke's extent is marked by the black lines. In the bottom figures, the state of excavation of the gold reef in December 2007 is indicated. Unmined areas are black and excavated areas white.

known for an accumulation of seismicity with larger magnitude compared to their surrounding (Gay & Ortlepp 1979; McGarr *et al.* 1975). Dykes are also known to bear higher compressive strength because they are stiffer than their surroundings (e.g. Zang & Stephansson 2010) and their initial stress state can be perturbed due to thermal stresses (Gay 1979). Therefore it is of interest in what distance from the dyke mining is possible without significantly increasing the probability of inducing an event in the dyke. We therefore apply a synthetic step-wise mining scenario, in which the excavation approaches the dyke from both sides until the dyke is reached; the actual mining compartments are not regarded here and in that sense the scenario is generic. To gain independence from a predefined slip direction, ΔCFS_{max} is applied for the elastic and the plastic analysis procedure. We use the orientation of the nodal plane N2 as well as for six additional planes that are slightly deviated from N2 to account for uncertainties in the resulting ΔCFS values (maximum deviation in strike direction is 20° and 10° in dip angle).

Figure 8 displays the increase of ΔCFS_{max} with the advancing excavation towards the dyke. The curve for the elastic stress transfer (black solid line) indicates that mining up to a distance of ∼120 m from the dyke is safe, since no changes in the ΔCFS_{max} are observed at the hypocentre of the seismic event. With decreasing distance to the dyke the ΔCFS_{max} value increases significantly up to a distance of ∼10 m from the dyke where the maximum of 31 MPa is reached. Quantitatively, the pseudo-plastic stress transfer curve (dashed black line) shows a similar but less extreme behaviour; the maximum ΔCFS_{max} value of 9 MPa is also at ∼10 m distance from the dyke.

Regardless the uncertainties and whether elastic or plastic analysis is used, this first-order assessment shows that small changes in the excavation distance with respect to the dyke, change the ΔCFS values significantly. However, at

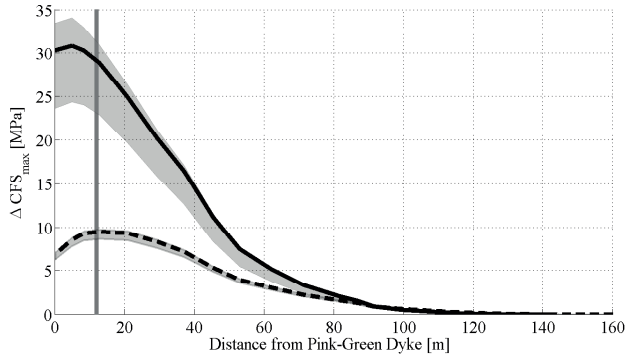

Fig. 8 The *seismic hazard mitigation* at the hypocentre of the M_w 1.9 seismic event. The $\Delta CFS_{max,el}$ for the actual rupture plane (solid line) and for deviated planes (shaded area) are displayed. In addition the same is displayed for $\Delta CFS_{max,pl}$ (dashed line) which is only computed from the vertical component of the stress tensor. Thereby a fully plastic dissipation of the horizontal stresses is assumed. The largest deviations of the plane's orientation from 348|56 in the strike are 20° and in the dip 10°. The vertical grey line indicates the actual approximate minimum distance of the mined out areas towards the dyke.

what level the ΔCFS value is critical is difficult to assess. This depends on (1) the stress state within the dyke before excavation, (2) the presence of pre-existing faults and their friction coefficient and (3) the rock strength of the intact rock. Furthermore, the real stress transfer is between the two end members of the elastic and the plastic case that we presented. Nevertheless, the definite increase clearly indicates that the hazard substantially increases within 50–10 m distance to the dyke.

6 Conclusion

In order to investigate the hypothesis that the M_w 1.9 seismic event on 27 December 2007 in the deep level Mponeng gold mine near Carletonville, South Africa, was induced by mining activity, a small scale ($\sim$0.05 km^3) 3D geomechanical-numerical model of the gold mine was built. The ΔCFS analysis of the modelled stress state, immediately before the seismic event, strongly indicates, that the stress changes by mining excavations induced this event. The rock was brought closer to failure on the derived rupture plane by stress changes of up to 1.5–15 MPa in dependence of the ΔCFS analysis type. The model uncertainties in the order of approximately $\pm$1 MPa do not change these principal findings. A forward modelling of a generic excavation scheme reveals that with decreasing distance to the dyke the ΔCFS values increase significantly. Hence even small changes in the mining progress can have a significant impact on the seismic hazard, i.e. the change of the occurrence probability of inducing an event of economic concern.

Acknowledgements The authors would like to thank AngloGold Ashanti for the kind permission to work and publish the data of the Mponeng gold mine, and the JAGUARS group for the provision of the data. The authors would like to thank two anonymous reviewers whose comments and suggestions helped to improve the manuscript. Furthermore, the authors would like to thank Lanru Jing for his comments on an earlier version of the manuscript. Figures 1, 2, 3 and 7 were generated with the Generic Mapping Tool (GMT) (Wessel *et al.* 2013). In Figure 1 SRTM3 V2 topographic data was used. The beachball plot in Figure 2 was realised with the software MoPaD (http://www.mopad.org) by Krieger & Heimann (2012). Previously published preliminary results presented in a conference proceeding (Ziegler *et al.* 2014) contain some erroneous results and misinterpretations and should no longer be used.

References

AngloGold Ashanti Limited. 2013. *Online Sustainability Report*. Newtown, South Africa: Available from: www.aga-reports.com.

Armstrong, R.A., Compston, W., Retief, E.A., Williams, I.S., & Welke, H.J. 1991. Zircon ion microprobe studies bearing on the age and evolution of the Witwatersrand triad. *Precambrian Res.*, **53**(3-4), 243–266.

Aswegen, G. van. 2008. Ortlepp Shears – dynamic brittle shears of S. A. goldmines. *In: ISS Int. South Africa*.

Bott, M.H.P. 1959. The Mechanics of Oblique Slip Faulting. *Geol. Mag.*, **96**(02), 109–117.

Brady, B.H.G., & Brown, E.T. 2004. *Rock Mechanics for Underground Mining*. 3 edn. Dodrecht Boston London: Kluwer Academic Publishers.

Byerlee, J. 1978. Friction of rocks. *Pure Appl. Geophys.*, **116**(4-5), 615–626.

Coward, M.P., Spencer, R.M., & Spencer, C.E. 1995. Development of the Witwatersrand Basin, South Africa. *Geol. Soc. London, Spec. Publ.*, **95**(1), 243–269.

Eriksson, P.G., Hattingh, P.J., & Altermann, W. 1995. An overview of the geology of the Transvaal Sequence and Bushveld Complex, South Africa. *Miner. Depos.*, **30**(2), 98–111.

Frimmel, H.E., & Minter, W.E.L. 2002. Recent developments concerning the geological history and genesis of the Witwatersrand gold deposits, South Africa. *Chap. 2, pages 17–45 of:* Goldfarb, R.J., & Nielsen, R.L. (eds), *Integr. Methods Discov. Glob. Explor. Twenty-First Century*, 1 edn. Society of Economic Geologists.

Gay, N. C., & Ortlepp, W. D. 1979. Anatomy of a mining-induced fault zone. *Geol. Soc. Am. Bull.*, **90**(1), 47.

Gay, N.C. 1979. The state of stress in a large dyke on E.R.P.M., Boksburg, South Africa. *Int. J. Rock Mech. Min. Sci. Geomech. Abstr.*, **16**(3), 179–185.

Gercek, H. 2007. Poisson's ratio values for rocks. *Int. J. Rock Mech. Min. Sci. Geomech.*, **44**(1), 1–13.

Hall, R.C.B., Els, B.G., & Mayer, J.J. 1997. The Ventersdorp contact reef; final phase of the Witwatersrand Basin, independent formation, or precursor to the Ventersdorp Supergroup? *South African J. Geol.*, **100**(3), 213–222.

Harris, R.A. 1998. Introduction to Special Section: Stress Triggers, Stress Shadows, and Implications for Seismic Hazard. *J. Geophys. Res.*, **103**(B10), 24347.

Hasegawa, H.S., Wetmiller, R.J., & Gendzwill, D.J. 1989. Induced seismicity in mines in Canada - An overview. *Pure Appl. Geophys.*, **129**(3-4), 423–453.

Haxby, W.F., & Turcotte, D.L. 1976. Stresses induced by the addition or removal of overburden and associated thermal effects. *Geology*, **4**(3), 181–184.

Heidbach, O., & Ben-Avraham, Z. 2007. Stress evolution and seismic hazard of the Dead Sea Fault System. *Earth Planet. Sci. Lett.*, **257**(1-2), 299–312.

Hofmann, G., Ogasawara, H., Katsura, T., & Roberts, D. 2012. An Attempt to constrain the Stress and Strength of a Dyke that accomodated a Ml 2.1 Seismic Event. *Pages 1–15 of: South. Hemisph. Int. Rock Mech. Symp. SHIRMS 2012*. The Southern African Institute of Mining and Metallurgy.

Hofmann, G., Scheepers, L., & Ogasawara, H. 2013. Loading conditions of geological faults in deep level tabular mines. *Pages 560–580 of:* Ito, Takatoshi (ed), *Proc. 6th Int. Symp. In-Situ Rock Stress*. Sendai: Tohoku University.

Horner, R.B., & Hasegawa, H.S. 1978. The seismotectonics of southern Saskatchewan. *Can. J. Earth Sci.*, **15**(8), 1341–1355.

Jaeger, J.C., Cook, N.G.W., & Zimmerman, R.W. 2007. *Fundamentals of Rock Mechanics*. 4th edn. Malden Oxford Carlton: Blackwell Publishing Ltd.

Jolley, S.J., Freeman, S.R., Barnicoat, A.C., Phillips, G.M., Knipe, R.J., Pather, A., Fox, N.P.C., Strydom, D., Birch, M.T.G., Henderson, I.H.C., & Rowland, T.W. 2004. Structural controls on Witwatersrand gold mineralisation. *J. Struct. Geol.*, **26**(6-7), 1067–1086.

Jones, M.Q.W. 1988. Heat flow in the Witwatersrand Basin and environs and its significance for the South African Shield Geotherm and lithosphere thickness. *J. Geophys. Res.*, **93**(B4), 3243–3260.

King, G.C.P., Stein, R.S., & Lin, J. 1994. Static stress changes and the triggering of earthquakes. *Bull. Seismol. Soc. Am.*, **84**(3), 935–953.

Krieger, L., & Heimann, S. 2012. MoPaD—moment tensor plotting and decomposition: a tool for graphical and numerical analysis of seismic moment tensors. *Seismol. Res. Lett.*, **83**(3), 589–595.

Kwiatek, G., & Ben-Zion, Y. 2013. Assessment of P and S wave energy radiated from very small shear-tensile seismic events in a deep South African mine. *J. Geophys. Res. Solid Earth*, **118**(7), 3630–3641.

Kwiatek, G., Plenkers, K., Nakatani, M., Yabe, Y., & Dresen, G. 2010. Frequency-Magnitude Characteristics Down to Magnitude -4.4 for Induced Seismicity Recorded at Mponeng Gold Mine, South Africa. *Bull. Seismol. Soc. Am.*, **100**(3), 1165–1173.

Leonard, M. 2010. Earthquake Fault Scaling: Self-Consistent Relating of Rupture Length, Width, Average Displacement, and Moment Release. *Bull. Seismol. Soc. Am.*, **100**(5A), 1971–1988.

Lindau, A. 2007. *Gravity Information System*. www.ptb.de/cartoweb3/SISproject.php. Online. Last accessed: 24 May 2013.

Lucier, A.M., Zoback, M.D., Heesakkers, V., Reches, Z., & Murphy, S.K. 2009. Constraining the far-field in situ stress state near a deep South African gold mine. *Int. J. Rock Mech. Min. Sci.*, **46**(3), 555–567.

Malan, D. F. 1999. Time-dependent Behaviour of Deep Level Tabular Excavations in Hard Rock. *Rock Mech. Rock Eng.*, **32**(2), 123–155.

MatWeb LLC. 2013. *MatWeb - Material property data*. http://www.matweb.com. Online. Last accessed: 10 April 2013.

McGarr, A. 1971. Violent deformation of rock near deep-level, tabular excavations—seismic events. *Bull. Seismol. Soc. Am.*, **61**(5), 1453–1466.

McGarr, A., Spottiswoode, S.M., & Gay, N.C. 1975. Relationship of mine tremors to induced stresses and to rock properties in the focal region. *Bull. Seismol. Soc. Am.*, **65**(4), 981–993.

Morris, A., Ferrill, D. A., & Henderson, D. B. 1996. Slip-tendency analysis and fault reactivation. *Geology*, **24**(3), 275.

Nakatani, M., Yabe, Y., Philipp, J., Morema, M., Stanchits, S., Dresen, G., & JAGUARS Research Group. 2008. Acoustic emission measurements in a deep gold mine in South Africa: Project overview and some typical waveforms. *Seismol. Res. Lett.*, **79**(2), 311.

Naoi, M., Nakatani, M., Yabe, Y., & Philipp, J. 2008. Very high frequency AE (up to 200 kHz) and microseismicity observation in a deep South African gold mine-evaluation of the acoustic properties of the site by in-situ test -. *Seism. Res. Lett.*, **79**(2), 330.

Naoi, M., Nakatani, M., Yabe, Y., Kwiatek, G., Igarashi, T., & Plenkers, K. 2011. Twenty Thousand Aftershocks of a Very Small (M 2) Earthquake and Their Relation to the Mainshock Rupture and Geological Structures. *Bull. Seismol. Soc. Am.*, **101**(5), 2399–2407.

Orlecka-Sikora, B., Lasocki, S., Lizurek, G., & Rudziński, Ł. 2012. Response of seismic activity in mines to the stress changes due to mining induced strong seismic events. *Int. J. Rock Mech. Min. Sci.*, **53**(July), 151–158.

Ortlepp, W.D. 1992. Note on fault-slip motion inferred from a study of micro-cataclastic particles from an underground shear rupture. *Pure Appl. Geophys.*, **139**(3-4), 677–695.

Ortlepp, W.D. 2001. Thoughts on the rockburst source mechanism based on observations of the mine-induced shear rupture. *In: Proc. 5th Int. Symp. Rockbursts Seism. Mines*. South African Institute of Mining and Metallurgy.

Plenkers, K., Kwiatek, G., Nakatani, M., & Dresen, G. 2010. Observation of Seismic Events with Frequencies f $>$ 25 kHz at Mponeng Deep Gold Mine, South Africa. *Seismol. Res. Lett.*, **81**(3), 467–479.

Poujol, M, Robb, L.J, & Respaut, J.P. 1999. U–Pb and Pb–Pb isotopic studies relating to the origin of gold mineralization in the Evander Goldfield, Witwatersrand Basin, South Africa. *Precambrian Res.*, **95**(3-4), 167–185.

Pretorius, D.A. 1976. The nature of Witwatersrand gold-uranium deposits. *Chap. 2, page 656 of:* Wolf, K.H. (ed), *Handb. Strat. Stratif. ore Depos. - Au, U, Fe, Mn, Hg, Sb, W P Depos. - Vol. 7*. Amsterdam Oxford New York: Elsevier Scientific Publishing Company.

Prinsloo, L. 2011. South African mine deaths down 24% in 2010. *Min. Wkly.*, **27**(January 2011).

Pytel, W. 2003. Rock mass—mine workings interaction model for Polish copper mine conditions. *Int. J. Rock Mech. Min. Sci.*, **40**(4), 497–526.

Robb, L. J., Davis, D. W., Kamo, S. L., & Meyer, F. M. 1992. Ages of altered granites adjoining the Witwatersrand Basin with implications for the origin of gold and uranium. *Nature*, **357**(6380), 677–680.

Roberts, M.K., & Schweitzer, J.K. 1999. Geotechnical areas associated with the Ventersdorp Contact Reef, Witwatersrand Basin, South Africa. *J. South African Inst. Min. Metall.*, **99**(2), 157–166.

Ryder, J.A. 1988. Excess shear stress in the assessment of geologically hazardous situations. *J. South African Inst. Min. Metall.*, **88**(1), 27–39.

Scoates, J.S., & Friedman, R.M. 2008. Precise age of the platiniferous Merensky Reef, Bushveld Complex, South Africa, by the U-Pb zircon chemical abrasion ID-TIMS technique. *Econ. Geol.*, **103**(May), 465–471.

Stanchits, S., Dresen, G., & JAGUARS Research Group. 2010. Formation of Faults in Diorite and Quartzite Samples Extracted From a Deep Gold Mine (South Africa). *Page 5605 of: Geophys. Res. Abstr.*, vol. 12.

Stein, R.S. 1999. The role of stress transfer in earthquake occurrence. *Nature*, **402**(6762), 605–609.

Van der Westhuizen, W.A., De Bruiyn, H., & Meintjes, P.G. 1991. The Ventersdorp supergroup: an overview. *J. African Earth Sci. (and Middle East)*, **13**(1), 83–105.

Wessel, P., Smith, W.H.F., Scharroo, R., Luis, J., & Wobbe, F. 2013. Generic Mapping Tools: Improved Version Released. *Eos, Trans. Am. Geophys. Union*, **94**(45), 409–410.

Yabe, Y., Philipp, J., Nakatani, M., Morema, G., Naoi, M., & Kawakata, H. 2009. Observation of numerous aftershocks of an Mw 1.9 earthquake with an AE network installed in a deep gold mine in South Africa. *Earth Planets Sp.*, **61**(10), 49–52.

Zang, A., & Stephansson, O. 2010. *Stress Field of the Earth's Crust*. Dordrecht: Springer Netherlands.

Ziegler, M., Reiter, K., Heidbach, O., Zang, A., Kwiatek, G., Dahm, T., Dresen, G., & Hofmann, G. 2014. Mining induced static stress transfer and its relation to a high-precision located Mw = 1.9 seismic event in a South African gold mine. *Pages 603–608 of:* Alejano, L.R., Perucho, A., Olalla, C., & Jiménez, R. (eds), *Rock Eng. Rock Mech. Struct. Rock Masses*. London: Taylor & Francis Group.